nature astronomy

Article

https://doi.org/10.1038/s41550-024-02206-x

Oxygen production from dissociation of Europa's water-ice surface

Received: 24 January 2023

Accepted: 17 January 2024

Published online: 04 March 2024

Check for updates

J. R. Szalay[1] ✉, F. Allegrini[2,3], R. W. Ebert[2,3], F. Bagenal[4], S. J. Bolton[2], S. Fatemi[5], D. J. McComas[1], A. Pontoni[2], J. Saur[6], H. T. Smith[7], D. F. Strobel[8], S. D. Vance[9], A. Vorburger[10] & R. J. Wilson[4]

Jupiter's moon Europa has a predominantly water-ice surface that is modified by exposure to its space environment. Charged particles break molecular bonds in surface ice, thus dissociating the water to ultimately produce H_2 and O_2, which provides a potential oxygenation mechanism for Europa's subsurface ocean. These species are understood to form Europa's primary atmospheric constituents. Although remote observations provide important global constraints on Europa's atmosphere, the molecular O_2 abundance has been inferred from atomic O emissions. Europa's atmospheric composition had never been directly sampled and model-derived oxygen production estimates ranged over several orders of magnitude. Here, we report direct observations of H_2^+ and O_2^+ pickup ions from the dissociation of Europa's water-ice surface and confirm these species are primary atmospheric constituents. In contrast to expectations, we find the H_2 neutral atmosphere is dominated by a non-thermal, escaping population. We find 12 ± 6 kg s^{-1} ($2.2 \pm 1.2 \times 10^{26}$ s^{-1}) O_2 are produced within Europa's surface, less than previously thought, with a narrower range to support habitability in Europa's ocean. This process is found to be Europa's dominant exogenic surface erosion mechanism over meteoroid bombardment.

Europa's interaction with its space environment, notably charged particles, ultraviolet light and meteoroid impacts, modifies its surface chemistry, leading to erosion and deposition of exogenic material. Charged particles dissociate H_2O in the surface ice (breaking molecular bonds), which subsequently recombine predominantly into molecular H_2 and O_2 (refs. 1,2). These molecular species are expected to be dominantly released from the surface by thermal desorption[2–4]. Thermal desorption along with sputtering from electrons[5] or ions[6,7] can liberate these molecules from the surface into Europa's atmosphere. This atmosphere is understood to comprise H (ref. 8) and H_2, O and O_2 (refs. 9–12), and H_2O (refs. 12–14). Atmospheric neutrals can become ionized as pickup ions (PUIs) that are incorporated into Jupiter's magnetospheric plasma[15–18]. Atmospheric sputtering, in which a plasma exchanges momentum with and erodes the neutral atmosphere, was originally proposed to be the dominant loss mechanism of neutral O_2[15]. Subsequently, electron impact ionization[3] and symmetric $O_2^+ \rightarrow O_2$ charge exchange[19] have also been proposed as the primary drivers of O_2 loss. H_2 loss has been less investigated theoretically; however, electron impact ionization is proposed to be its dominant loss mechanism[3].

The atmosphere is understood to consist of thermally desorbed molecules. It is governed by the surface temperature[20] as well as a directly sputtered source[21]. Although Galileo's E4 and E6 fly-bys at

[1]Department of Astrophysical Sciences, Princeton University, Princeton, NJ, USA. [2]Southwest Research Institute, San Antonio, TX, USA. [3]Department of Physics and Astronomy, University of Texas at San Antonio, San Antonio, TX, USA. [4]Laboratory for Atmospheric and Space Physics, University of Colorado Boulder, Boulder, CO, USA. [5]Department of Physics, University of Umeå, Umeå, Sweden. [6]Institute of Geophysics and Meteorology, University of Cologne, Cologne, Germany. [7]The Johns Hopkins University Applied Physics Laboratory, Baltimore, MD, USA. [8]The Johns Hopkins University, Baltimore, MD, USA. [9]Jet Propulsion Laboratory, California Institute of Technology, Pasadena, CA, USA. [10]Physics Institute, University of Bern, Bern, Switzerland. ✉e-mail: jszalay@princeton.edu

https://doi.org/10.1038/s41550-024-02206-x

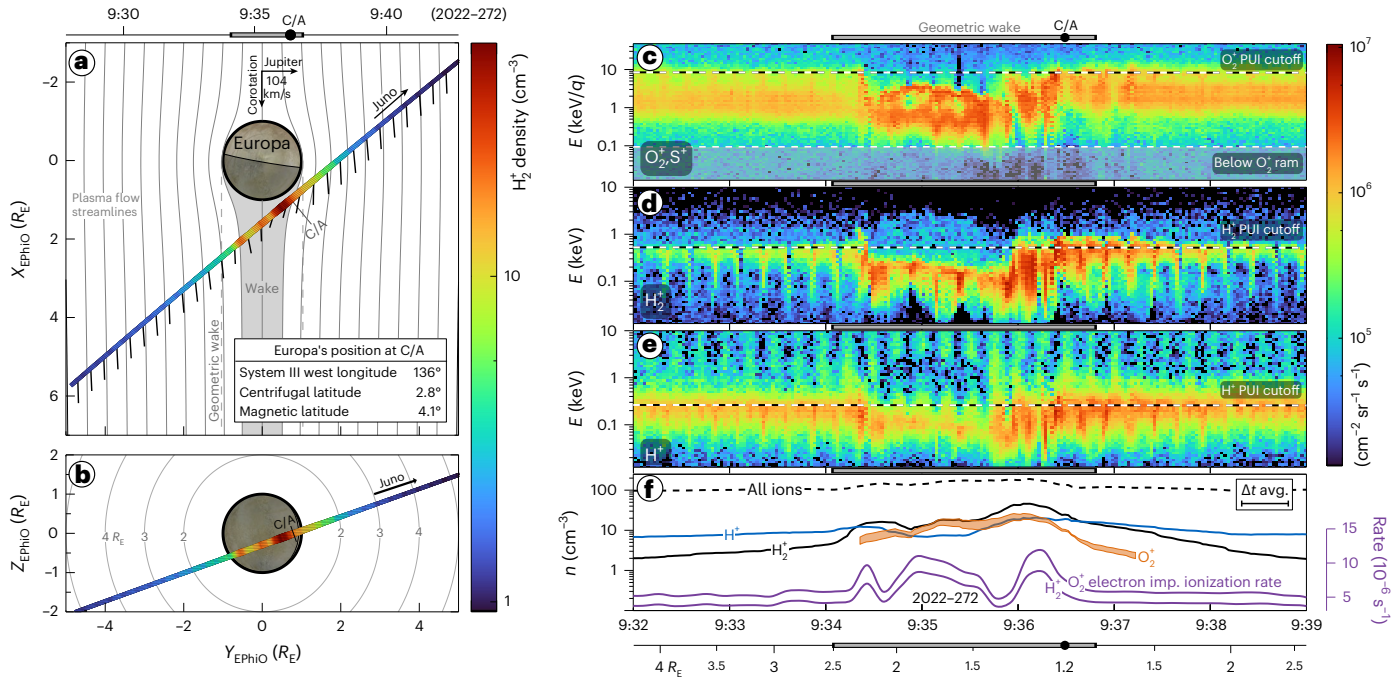

Fig. 1 | Overview of Europa fly-by and plasma observations. a,**b**, Density of H_2^+ PUIs directly picked up from Europa's neutral atmosphere for X_{EPhiO} (**a**) and Z_{EPhiO} (**b**). Velocity arrows indicate the plasma velocity vector as determined from proton observations, with the rigid corotation of 104 km s^{-1}. $R_E \equiv 1{,}560.8$ km is Europa's radius. Streamlines and associated wake are from an analytic model (Methods). **c**–**e**, Fluxes of O_2^+ and S^+ (**c**), H_2^+ (**d**) and H^+ (**e**) from JADE's TOF product. Horizontal dashed lines indicate the ram energy for O_2^+ (**c**) and cutoff energies (**c**–**e**) for PUIs assuming rigid corotation (Methods). **f**, Densities of individual species (orange, black and blue), all ions (dashed black) and electron impact ionization rates (purple, right axis). The altitude is shown underneath **c**–**f**. The boundaries of the geometric wake are shown with horizontal grey bars above or below each panel. Juno's close approach (C/A) was on 2022-272 9:36:29. Each horizontal tick corresponds to 1 min. avg., average; imp., impact.

close-approach altitudes of 692 and 586 km inferred the presence of PUIs near Europa, instrumental limitations prevented a compositional deconvolution of the measured plasma into magnetospheric and Europa-genic material[22]. Additionally, several species of PUIs were inferred from ion-cyclotron emissions during the E11 and E15 fly-bys[23]. Constraints on the relative abundances of Europa's atmospheric neutral and plasma species were previously derived primarily from remote-sensing ultraviolet observations. As there had been no direct in situ particle observations of Europa-genic material composition in the moon's vicinity, the composition of Europa's atmosphere, how much of it is lost and how much plasma Europa contributes to Jupiter's magnetosphere remained unresolved[24].

Observations and PUI characteristics

The Juno mission[25] is equipped with the Jovian Auroral Distributions Experiment (JADE)[26], which includes several electron analysers and a time-of-flight (TOF) ion mass spectrometer. JADE's ion instrument measures the energy and angle distributions of positively charged particles with an energy per charge (E/q) of 10 to 46 keV/q. Juno performed a fly-by of Europa on 29 September 2022 (day of year 272), with its closest approach at 9:36:29 UTC at an altitude of 353 km and a radial distance of 1.2 R_E, where 1 R_E = 1,560.8 km. Relevant orbital parameters are given in Extended Data Table 1. Figure 1a,b shows the fly-by trajectory in Europa phi orbital (EPhiO) coordinates, where +z is aligned with Jupiter's rotation axis, +y is the direction of the component of the Europa–Jupiter vector perpendicular to +z and +x completes the right-handed system, which is aligned with the rigid corotation direction.

Juno transits the geometric wake from 9:34:06 to 9:36:48 UTC with a speed relative to Europa of 23.6 km s^{-1}. Figure 1c–f shows plasma observations from JADE. The fluxes are derived by integrating the TOF data to identify H^+, H_2^+, and O_2^+/S^+ (Methods) to focus on Europa-genic PUI species. The upstream densities of ~100 cm^{-3} at Europa during this fly-by are within the 25–50% range of densities observed over Galileo's tour[27]. This plasma density contrasts with Galileo's E4 fly-by, which had a similar fly-by geometry, but with much lower upstream total ion densities of ~20 cm^{-3} (ref. 22). It also contrasts with Galileo's E12 fly-by when Europa was near the plasma sheet. Its plasma waves spectrometer observed large densities >600 cm^{-3} before the transit, and <200 cm^{-3} after. However, this enhancement may have been due to activity at Europa[28], and the E12 density profile is markedly different than that observed during Juno's Europa fly-by.

The expected PUI cutoffs (Methods) for rigid corotation of 104 km s^{-1} at Juno are 0.3, 0.5 and 8 keV for H^+, H_2^+ and O_2^+, respectively, as shown in the horizontal dashed lines in Fig. 1c–e, which also shows the ram energy for O_2^+ of 90 eV. Ram energies for the hydrogen species are below JADE's 10 eV/q lower limit for ions. Most notably for H_2^+ and O_2^+, the cutoff in fluxes at the higher-energy range matches almost identically to the expected PUI cutoff (for rigid corotation) outside the Europa transit. Just after crossing into the wake, Juno transits a region with a varying PUI cutoff energy, indicating these ions were picked up at speeds differing from rigid corotation. This corresponds to the speed increasing around the flanks of Europa and the slowing and deflection of plasma within its wake.

Several species from distinct plasma populations have been observed near Europa. JADE can discriminate these with its TOF observations (Fig. 2). Magnetospheric H^+, O^{2+}, S^{3+}, O^+/S^{2+} and S^+ are observed consistently throughout the encounter above a few kilo-electronvolts, with a depletion below these energies within Europa's wake. Notably, S^{3+} at M/q = 10.67 (atomic mass unit per elementary charge) is an important tracer for magnetospheric plasma as there is no appreciable source of sulfur from Europa compared to the Io-genic plasma dominating the magnetosphere. In contrast, H_2^+ of Europa-genic origin is more prominently observed closer to Europa where the magnetospheric plasma populations are depleted. For O^+, both Europa-genic ions near the PUI

https://doi.org/10.1038/s41550-024-02206-x

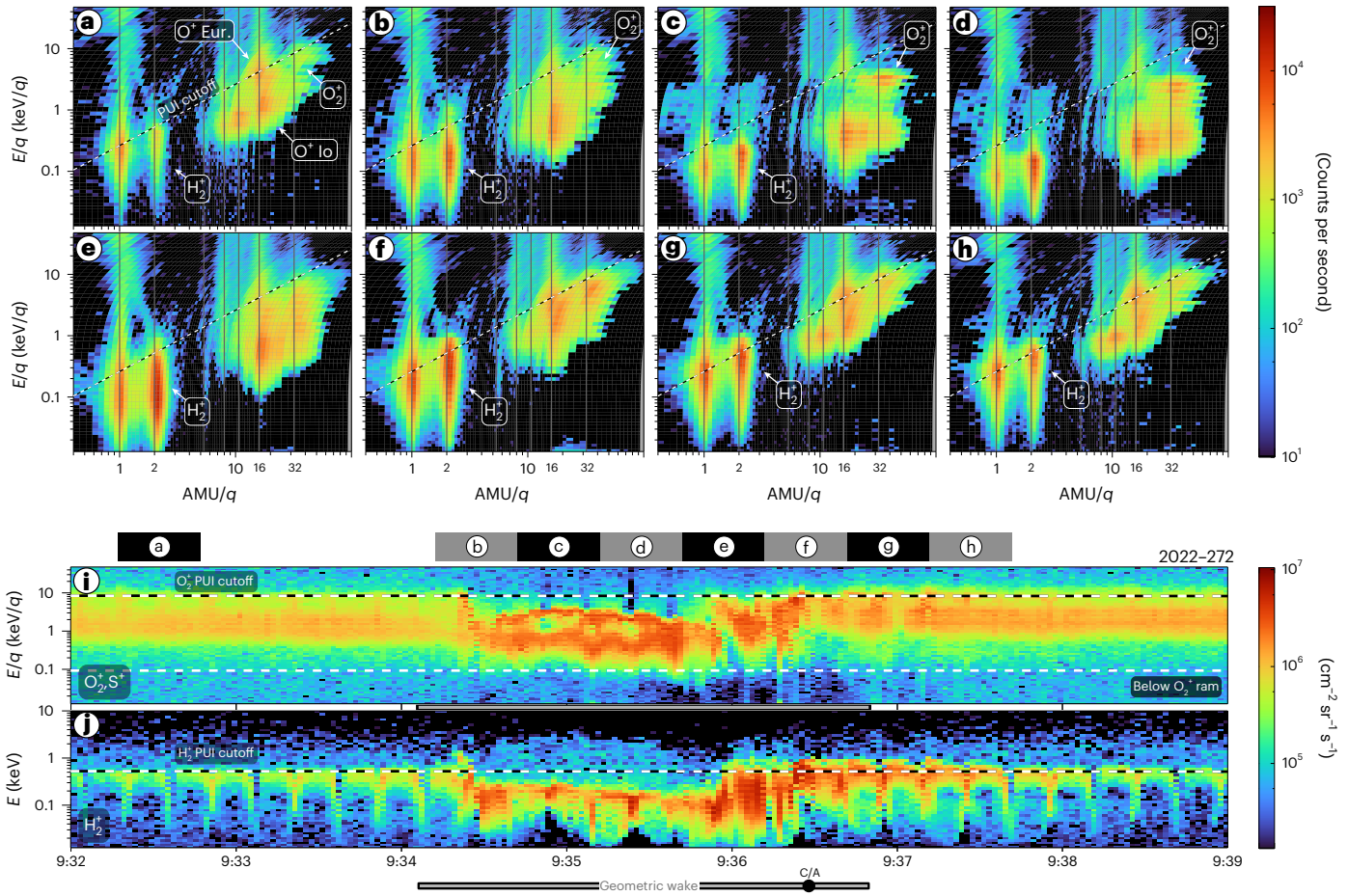

Fig. 2 | Ion composition for eight periods along the fly-by. a–h, Average ion count rates as a function of energy per charge and mass per charge. The diagonal line on each shows the cutoff for locally picked up ions assuming that they are picked up at a rigid corotation speed of 104 km s^{-1} relative to Europa (Methods). The corresponding 30 s intervals are indicated on the top of **i**. **i**,**j** The same as shown in Figs. 1c (**i**) and 1e (**j**).

cutoff energy and Io-genic O^+ near the corotation speed are observed. For example, Fig. 2a shows both O^+ populations separated by energy. The expected Europa plasma torus H_2^+ densities at Europa's orbit are 0.2–0.3 cm^{-3} (ref. 29), which are negligible compared to the H_2^+ densities of ~2–60 cm^{-3} observed here.

Near Europa there are two distinct ion populations in the $M/q = 32$ fluxes that separate in energy. We attribute the lower-energy population to magnetospheric ions and the higher-energy population to O_2^+ PUIs. Before and after the encounter, there is a quasi-steady-state population peaking in differential energy flux between 1 and 10 keV. These fluxes probably contain a mixture of both magnetospheric S^+ ions originating from Io as well as Europa-genic O_2^+ PUIs near the PUI cutoff energy observed inside and outside Europa's orbit. They may also contain a lower level of false coincidences from O^+ and S^{++} with longer TOFs on the lower end of this energy range. Within the wake, an enhancement is observed in $M/q = 32$ fluxes. The magnetospheric O^{n+} and S^{n+} are all slowed within the wake and observed with lower energies. The higher-energy population in the wake, notably ~2–3 keV/q with $M/q = 32$, follows very closely to the H_2^+ PUI population. If both species were picked up in identical locations and transport conditions, the O_2^+ PUIs would have a similar energy distribution upscaled by a factor of 16 in energy for the difference in mass between O_2 and H_2, with the exception of additional gyrotropic effects discussed below. As the $M/q = 2$ fluxes are unambiguously H_2^+ PUIs from Europa, we can use their temporal and energy distribution to constrain Europa-genic O_2^+ (Extended Data Fig. 1). Figure 1f shows the range of derived O_2^+ densities during the period when the $M/q = 32$ energy-per-charge spectrogram (Fig. 1c) is distinct from the upstream conditions, specifically from 2022-272 9:34:20 to 9:37:15. As densities derived for the full $M/q = 32$ product would contain contributions from several species, we isolate and show only the O_2^+ densities we can derive in this data-driven way. Unlike at Ganymede, where H_3^+ was observed[30], probably being a direct by-product of a relatively dense H_2 atmosphere, no appreciable signatures of H_3^+ were observed during this Europa transit. These observations also provide in situ constraints on PUI currents, the subtraction of which is necessary to better constrain the induced current due to Europa's subsurface ocean[31].

Some of the differences between the H_2^+ and O_2^+ energy distributions may be due to gyrotropic effects[32]. For an average upstream magnetic field magnitude of ~440 nT using the JRM09 internal field model[33] and current sheet model[34] and assuming pickup at a rigid corotation of 104 km s^{-1}, the gyroradius for H_2^+ is ~5 km whereas the O_2^+ gyroradius is ~80 km. With a speed relative to Europa of 23.6 km s^{-1}, Juno transits a full O_2^+ gyroradius every 3–4 s, or two ion measurement periods at 2 s each such that JADE may not be sampling a fully gyrotropic population at any given period, particularly near a close approach where these ions would be the most freshly picked up.

Within the geometric wake, the dominant Europa-genic species are H_2^+ and O_2^+, with both densities peaking ~30 s before close approach. This confirms that the primary atmospheric neutral constituents are H_2 and O_2. With the exception of when Juno was most central to the wake at ~9:35, the O_2^+ densities are lower than those observed for H_2^+. However, Juno may have missed the densest core of O_2^+ in Europa's

https://doi.org/10.1038/s41550-024-02206-x

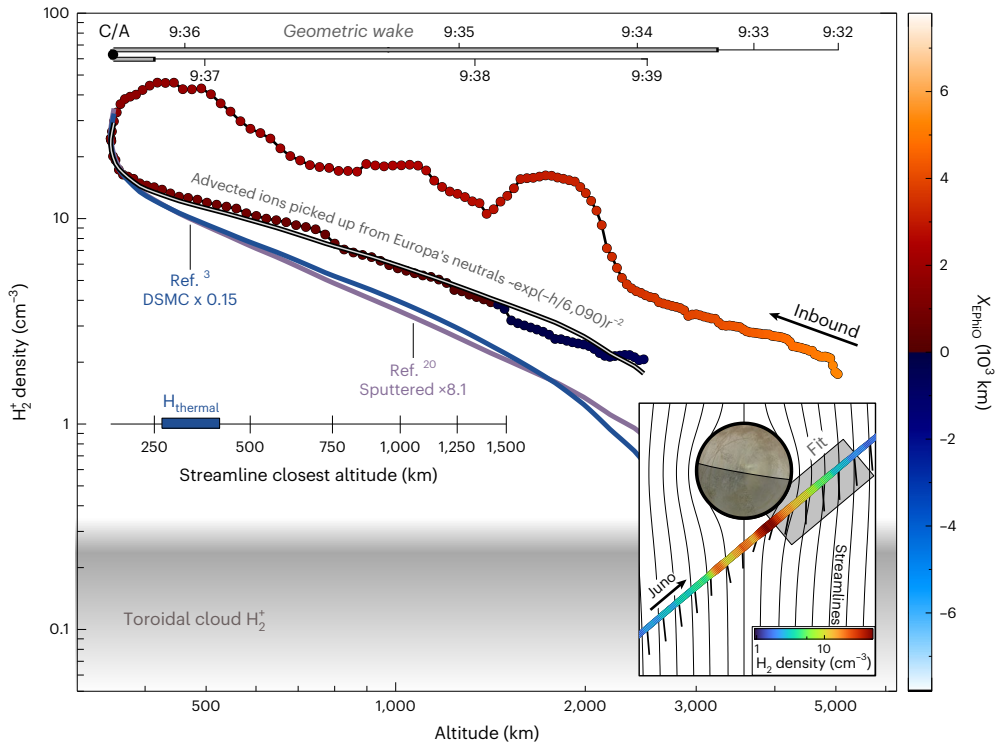

Fig. 3 | Altitude profile for H_2^+ PUIs. H_2^+ density coloured by X_{EPhiO} such that densities observed upstream from the centre of Europa are blue and are red or orange downstream. The outbound portion of the trajectory, 'Fit' in the inset, is compared to a PUI advection solution (Methods). Overlaid curves show PUI densities corresponding to the advection solution for a PUI population from: (1) an ionized neutral atmosphere varying as $\exp(-h/\lambda)r^{-2}$ where $\lambda = 6{,}090 \pm 890$ km (grey), (2) scaled from a comprehensive DSMC atmosphere model (blue)[3] and (3) scaled from a sputtered-only model (purple)[20]. The grey region at the bottom shows the expected density of Europa-genic H_2^+ PUIs already incorporated into Jupiter's magnetospheric plasma[29].

wake[16] due to its fly-by trajectory and three-dimensional nature of the streamlines carrying PUIs.

Juno encountered a diverse and mixed plasma environment with Europa-genic PUIs and magnetospheric plasma at all altitudes visited. The relative ratios of the various constituents vary substantially, such that this convection-driven ionosphere is compositionally stratified. Thus, a meaningful scale height cannot be derived from a single electron density observation[35]. This finding also has important implications for upcoming Europa Clipper and Jupiter Icy moons Explorer (JUICE) fly-bys. Specifically, the energy-per-charge observations with Clipper's Faraday cup[36] will need to be carefully interpreted given the overlap of O_2^+ PUIs with magnetospheric S^+.

Atmospheric properties

The observed PUIs can be used to infer atmospheric neutral densities. To do so, we focus on times when Juno was on the Jupiter-facing side of the geometric wake (Fig. 3 inset). This location is where Juno transits streamlines that have the nearest access to the densest portions of the neutral atmosphere, which reduces additional effects due to the complex wake dynamics and enables us to estimate total atmospheric neutral densities upstream along streamlines connected to Juno using a small number of realistic assumptions (Methods). We calculate the electron impact ionization rates (Methods and Extended Data Fig. 2) for all JADE data near Europa's orbit (Extended Data Table 2 and Extended Data Fig. 3) and during the fly-by (Extended Data Fig. 4), finding this mechanism to be the dominant ionizing process for these neutrals at Europa (Extended Data Table 3), as shown in Fig. 1f. From these rates, we compare modelled PUI densities from an advection model (Methods and Extended Data Figs. 5 and 6) for three specific atmospheric neutral profiles to the H_2^+ densities in Fig. 3: (1) an analytic modified power-law distribution, (2) scaled to the published densities from a direct simulation Monte Carlo (DSMC) simulation that comprehensively simulates the entire thermal and sputtered neutral atmosphere[3] and (3) scaled to a solely sputtered source[20].

We find that a neutral atmospheric H_2 density profile $n(r) = n_0 \exp(-h/\lambda)r^{-2}$ (ref. 37) is able to reproduce the observed PUI density profile. Using a χ^2 fit, we find that the surface density $n_0 = 1.8 \pm 0.05 \times 10^5$ cm^{-3} and $\lambda = 6{,}090 \pm 890$ km fit the JADE PUI observations. Both the DSMC full-atmosphere simulation and sputtered-only simulation, when scaled with the JADE data to their peak expected densities, underpredict the radial profile of observed H_2^+ PUIs. This finding is insensitive to a reasonable range of streamline model parameters (Methods). In addition to being the dominant ionizing process, electron impact ionization is found to be the overall dominant loss mechanism for H_2 at Europa's orbital distance within Jupiter's magnetosphere. Using these neutral profiles with our derived electron impact ionization rates, we find the total atmospheric loss rate as PUIs (Methods) to be 0.16 ± 0.04 kg s^{-1} ($4.8 \pm 0.1 \times 10^{25}$ s^{-1}). Comparing with previous H_2^+ ion observations in Jupiter's magnetosphere[29], we infer 6–41% of Europa's escaping H_2 neutrals are directly lost from the atmosphere as H_2^+ PUIs (Methods). Much of the remaining atmospheric losses will be in the form of neutrals, which populate a neutral toroidal cloud co-orbiting with Europa[3,29,38–40]. This process should also be occurring to varying degrees at Ganymede[41] and Callisto[42]. An even smaller fraction would leave the Jovian system as unbound energetic neutral atoms[38].

In the dawn-side region, we estimate Juno to be connected to streamlines that probe to less than 250 km altitude (inset axis in Fig. 3). H_2 neutrals with a thermal speed distribution driven by Europa's 86–132 K surface temperatures[43] would have scale heights of 270–415 km. Hence, we can assess from our advection analysis the total content of the neutral atmospheric H_2 population within a single thermal scale height. The finding that a profile of $n(r) = n_0 \exp(-h/\lambda)r^{-2}$

https://doi.org/10.1038/s41550-024-02206-x

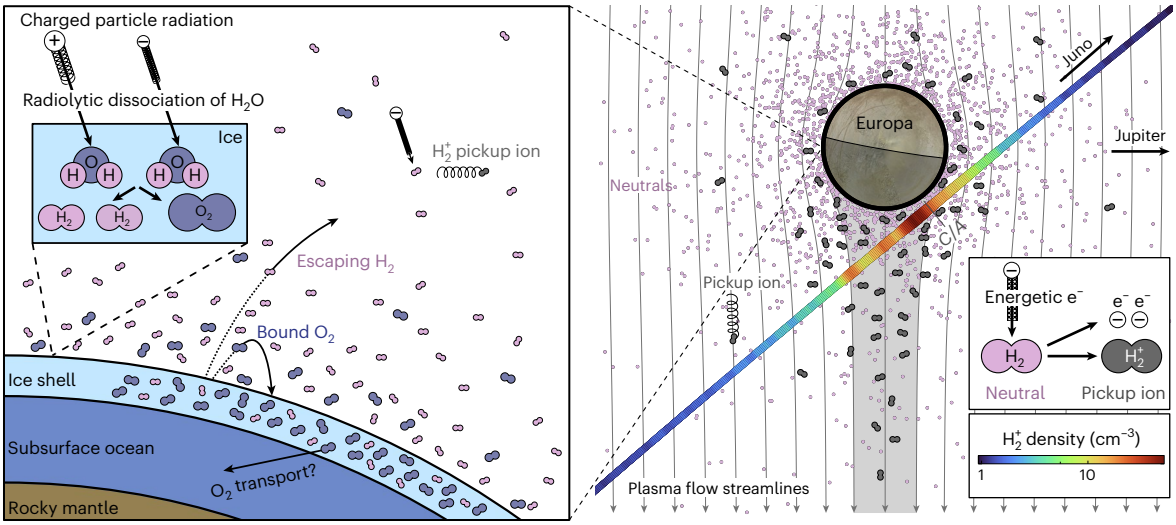

Fig. 4 | Overview of Juno's Europa fly-by. Water ice on the surface of Europa is dissociated by radiolysis to form O_2 and H_2. These gases can migrate both inwards towards the subsurface ocean or escape the surface by thermal desorption or direct sputtering to form its atmosphere. The lighter H_2 occupies a more extended region than heavier O_2, which remains closer to the surface. A portion of the neutrals in the atmosphere are ionized and picked up by the magnetospheric plasma. Juno observes these PUIs, with the relative abundances driven by the various processes described here. The radiolysis dissociation inset was adapted from ref. 2. Particles shown are O_2 (blue), H_2 (pink) and H_2^+ (grey).

can fit the observed PUIs suggests the atmospheric neutral population is not thermalized. This is also supported by comparison with the full-atmosphere DSMC simulation from ref. 3, which is dominated by thermalized neutrals and is not consistent with the observations. Such a finding is contrary to the prevailing understanding before the Juno fly-by that H_2 neutrals in the atmosphere would have all three of the following properties: (1) They predominantly leave the surface with a thermal speed distribution closely matching the local temperature of the surface[2]. (2) They have small scale heights ~270–415 km. (3) Their speed distribution is not further modified. Additionally, the comparison in Fig. 3 with a sputtered-only model[20] shows the observed population is also not consistent with a completely sputter-driven population. The radial profile we find, which is steeper than r^{-2}, indicates that there is a predominantly escaping neutral population, which would follow r^{-2}, that is also being ionized and depleted to steepen the radial neutral profile, as discussed in the next section.

The vertical neutral atmospheric column density (Methods) along the radial direction from the centre of Europa is calculated to be $1.8 \pm 0.1 \times 10^{13}$ cm^{-2} for H_2 from the inferred non-thermal neutral population. Before Juno's fly-by, this value had not been observationally constrained[7]. The H_2 column densities derived here are a factor of ~4 smaller than those estimated from ref. 3 of 7.7×10^{13} cm^{-2}, comparable to the value from ref. 21 of 2.5×10^{13} cm^{-2} and an order of magnitude higher than the sputtered-only value from ref. 20 of 1.9×10^{12} cm^{-2}.

Unlike for H_2, for which the thermal neutral scale heights are comparable to Juno's fly-by altitudes, the expected scale heights for O_2 are tens of kilometres (refs. 4,20). Due to this, we do not derive the total loss rate of O_2 directly from the O_2^+ observations as we have done for H_2. PUIs from the denser thermal O_2 atmosphere may be highly concentrated in the most central portion of the wake and Juno may not have directly observed PUIs from this portion of the atmosphere. Therefore, we do not derive properties of the O_2 neutral atmosphere. However, the Juno fly-by still reveals important information about the evolution of neutral O_2. Electron impact ionization rates of 1.9×10^{-6} s^{-1} have been previously used to calculate modelled O_2 losses[15]. The electron impact ionization rates derived here of 4.9×10^{-6} s^{-1} upstream from 9:37 to 9:39 during the fly-by are a factor of ~3 larger, and those in the wake of $3.3–8.1 \times 10^{-6}$ s^{-1} are a factor of 2–4 times larger (Methods and Extended Data Table 3). The rate is proportional to the 1,356 Å O I emission rate used to derive the neutral column densities, which implies that this rate, at least for the time of the Juno fly-by, is also a factor of 2–4 larger. Consequently, to be consistent with brightness values measured remotely, we expect the O_2 atmosphere to be a factor of ~2–4 times less dense compared to estimates using pre-Juno electron impact dissociation rates. Hence, the Juno fly-by observations are consistent with a lower O_2 loss rate, both in the O_2 electron impact ionization rates and the H_2 loss rates that are a tracer for total O_2 production.

Discussion and conclusions

From a combination of Juno's Europa fly-by and several transits through Europa's orbit, we estimate Europa's total neutral H_2 loss rate to be 1.5 ± 0.8 kg s^{-1} ($4.5 \pm 2.4 \times 10^{26}$ s^{-1}). H_2 is an effective tracer for the evolution of Europa's surface ice. Observations of H_2^+ PUIs during Juno's single fly-by of Europa and of H_2^+ PUIs throughout Jupiter's magnetosphere taken over several years provide very similar loss rate estimates (Methods). Assuming that all oxygen produced by the radiolytic dissociation of H_2O in the surface forms molecular O_2 (ref. 1) and that the same process creating H_2 produces O_2 in a 2:1 ratio, we expect 12 ± 6 kg s^{-1} ($2.2 \pm 1.2 \times 10^{26}$ s^{-1}) of O_2 to be produced in the top layer of Europa's icy surface. This puts direct observational constraints on the pathways for O_2 produced in the surface, such as the total loss rate of O_2 from the atmosphere and O_2 accessible to the subsurface ocean. Figure 4 and Table 1 summarize the surface processes and Juno observations made during its fly-by of Europa.

Due to radiolysis, the loss rates of H_2 we derive require 13 ± 7 kg s^{-1} of water ice to be dissociated, which erodes Europa's surface by 1.5 ± 0.8 cm Myr^{-1} (95 ± 52 Myr m^{-1}). Galileo's observations of impact ejecta from its Europa fly-bys[44] were consistent with an impact ejecta mass loss of 0.2 kg s^{-1}, corresponding to an erosion rate of 0.2 mm Myr^{-1}, assuming that pure ice is ejected, which is more than an order of magnitude lower than that from the radiolysis-driven dissociation of surface ice calculated here. Additionally, as the top 30 cm of the surface is anticipated to be impact gardened over tens of millions of years (ref. 45), even with the modest H_2O loss rates derived here, the radiolysis-driven erosion of the surface is comparable to, if not the dominant driver of, Europa's surface erosion and modification. These updated constraints also affect the preservation of potential biosignatures in Europa's near-surface ice layers[46].

Historically, the neutral H_2 atmosphere was understood to be dominated by a thermalized population with a speed distribution like that of the local surface temperature[2,4]. In contrast to expectations, we

https://doi.org/10.1038/s41550-024-02206-x

Table 1 | Relevant parameters derived from Juno data

Parameter	Value
Europa's surface ice	
H_2 production	$1.5\pm0.8\,kg\,s^{-1}$ ($4.5\pm2.4\times10^{26}\,s^{-1}$)
O_2 production	$12\pm6\,kg\,s^{-1}$ ($2.2\pm1.2\times10^{26}\,s^{-1}$)
H_2O dissociation	$13\pm7\,kg\,s^{-1}$ ($4.5\pm2.4\times10^{26}\,s^{-1}$)
Surface erosion	$1.5\pm0.8\,cm\,Myr^{-1}$ ($95\pm52\,Myr\,m^{-1}$)
Europa's H_2 atmosphere	
H_2 profile	$n(r) = n_0 e^{-h/\lambda} r^{-2}$
H_2 surface density	$n_0 = 1.8\pm0.05\times10^5\,cm^{-3}$
H_2 ionization scale height	$\lambda = 6{,}090\pm890\,km$
H_2 outflow speed	$58\pm34\,m\,s^{-1}$
H_2 loss	$1.5\pm0.8\,kg\,s^{-1}$ ($4.5\pm2.4\times10^{26}\,s^{-1}$)
Direct H_2^+ loss	$0.16\pm0.04\,kg\,s^{-1}$ ($4.8\pm0.1\times10^{25}\,s^{-1}$)

In the H_2 profile relation, h is the altitude above the surface and r is the radial distance from Europa's centre.

find the neutral H_2 atmosphere is dominated by a non-thermal population with a radial dependence of $n(r) = n_0 \exp(-h/\lambda) r^{-2}$, as has been employed for Io's atmospheric escape[37]. Such a radial distribution would arise from an outflowing, escaping neutral population (r^{-2} dependence) that incurs losses ($\exp(-h/\lambda)$ dependence), which is directly observed for the $H_2 + e^- \rightarrow H_2^+ + 2e^-$ pathway as PUIs. From this altitude profile (Fig. 3), we find the average neutral outflow speed is $58 \pm 34\ m\ s^{-1}$. We independently estimate the total neutral outflow loss (Methods), which nearly identically matches the values derived relying primarily on Europa-genic H_2^+ PUI observations far from Europa[29]. Therefore, the H_2 neutral altitude profile and the total derived H_2 loss rates are independently consistent, giving further confidence that the H_2 population is non-thermal and has been heated after release from the surface by an additional mechanism. Although we cannot address the heating mechanism for such a population with this current analysis, it may be the result of atmospheric sputtering[15], direct surface sputtering[20,21], Joule heating[47] or a combination of these effects. Joule heating is a favourable candidate, as such a process is most efficient when the interaction strength (Methods) $\bar{\alpha} = 0.5$ (ref. 48), and we have found $\bar{\alpha} = 0.55$ to represent the observations well.

The overall budget of $12 \pm 6\ kg\ s^{-1}$ total O_2 produced in the surface is partitioned into atmospheric loss and potential sequestration into the surface ice. The loss of neutrals from the surface is often termed the 'source rate' in the literature, which is equal to the production rate if all neutrals eventually make their way to the surface or is less than the production rate if an appreciable fraction of neutrals are transported downward away from the surface. Before Juno's transit of Europa, model-driven estimates for the total Europa-genic O_2 source extended over two orders of magnitude[2,7,20,49] from 5 to 1,100 $kg\ s^{-1}$. Here, we constrain this value to less than $12 \pm 6\ kg\ s^{-1}$, as the production rate is an upper limit on the atmospheric source rate and is in the very lowest range of previous estimates. Previous modelling efforts provide context to the relative magnitude of oxygen production. A modelling study investigating the physics of O_2 production and ejection from the surface found production rates of 8–26 $kg\ s^{-1}$ to be consistent with O_2 forming a thin layer near the surface, compared to 430–1,100 $kg\ s^{-1}$ for a thick layer, for which the oxygen reservoirs exist deeper than the penetration depth of magnetospheric ions[7]. As the thin-layer hypothesis and corresponding modelled production rates are similar to the observational constraints found here, these results are consistent with the notion proposed by ref. 7 that oxygen could reside in a narrow layer near the surface. A separate modelling parameter study[16] showed that with upstream densities of 100 cm^{-3} like those observed on the Juno fly-by, our production rates of $12 \pm 6\ kg\ s^{-1}$ are consistent with Europa having a small height for neutral O_2 of approximately tens of kilometres.

With respect to potential transport downward and away from the surface, radiolytically produced O_2 retained in Europa's ice may work its way into the ocean as a possible source of metabolic energy for life[50]. Estimates of current O_2 delivery from the oxygenated ice to the liquid ocean range from 0.3 to 200 $kg\ s^{-1}$ (ref. 51) up to 300 $kg\ s^{-1}$ (ref. 52). Unless Europa's oxygen production was significantly higher in the past, the O_2 production rates found here of less than the 18 $kg\ s^{-1}$ available to be retained in Europa's surface ice provide a narrower range to support habitability than previous model-driven estimates.

Methods

PUI energy

PUIs are injected at a velocity in the corotating frame of $\mathbf{v}_{PUI,cor} = \mathbf{v}_{cor} - \mathbf{v}_{orb}$, where $v_{cor} = \omega r \cos\theta$ is the corotational speed, r is the radial distance, $v_{orb} = \sqrt{\mu/r}$ is the orbital speed, $\omega = 1.757 \times 10^{-4}\ s^{-1}$ is Jupiter's angular rotation frequency (period of 9.93 h), $\mu = 1.267 \times 10^{17}\ m^3\ s^{-1}$ is Jupiter's standard gravitational parameter and θ is the latitude. In a reference frame centred on Jupiter but not rotating with the planet, PUIs have a speed in the range from $v_{PUI,inj} = |2\mathbf{v}_{cor} - \mathbf{v}_{orb}|$ to $v_{PUI,min} = v_{orb}$. Juno's relative motion plays a role in the detected PUI energies. Hence, the peak observed speed expected in the spacecraft frame for PUIs is $v_{PUI,Juno} = |\mathbf{v}_{PUI,inj} - \mathbf{v}_{Juno}| = |\mathbf{v}_{Juno} - 2\mathbf{v}_{cor} + \mathbf{v}_{orb}|$, where $\mathbf{v}_{Juno}$ is the velocity vector of the Juno spacecraft with respect to Jupiter's centre in a non-rotating frame.

Density determination from TOF data by mass range

Although JADE's TOF product does not have directionality information, it does observe the full sky each ~30 s spin. We calculate partial numerical densities from the count rates as a function of energy over the JADE energy band-pass for each sample period of 2 s and apply a sliding average over a full 30 s spin. After all foregrounds and backgrounds are subtracted (see Supporting Information in ref. 29), we sum count rates over all TOFs corresponding to M/q between the mass ranges 1.5–2.5 for H_2^+ and 26–70 for O_2^+ and S^+ to determine a total count rate R_{obs} as a function of energy. Count rates for H^+ are derived from existing proton foreground removal methods used to isolate H_2^+. For all species-specific count rates, we subtract the average count rates per energy in the M/q range of 2.75 to 5.1 to remove the long TOF tail from O^+ and S^{++} ions that are foreground to other mass ranges (Supporting Information in ref. 29).

JADE instantaneously observes an angular range of 270° extending from the anti-sunward spin axis, such that for each spacecraft rotation, it records counts from a total angular extent of 6π sr, double-counting half the sky. We must reduce R_{obs} by an appropriate factor to determine the 'true' average count rate $R = \eta R_{obs}$ corresponding to the 4π sr full sky. Due to the instrument mounting and orbit geometry, for each observation by JADE, the plasma incident on JADE is predominantly observed on the hemisphere where JADE double-counts incident populations, which also gives improved counting statistics. Following previous analyses[29], we use $\eta = 0.5$.

We then convert count rate R into phase space density f using $f(v) = R/(G^v_{eff}(v)\, v^4)$, where $G^v_{eff} = G^E_{eff}/2$ is the energy-dependent geometric factor[53], with a factor of two between the energy geometric factor and velocity geometric factor[54], and v is the measured energy per charge converted to speed for each given species mass. In turn, the number density derived from a one-dimensional phase space density is $n_{num} = 4\pi \int_0^\infty f(v)\, v^2\, dv$. For JADE data with count rates in discrete energy bins, the numerical partial number density is given by $n_{num} = (4\pi/3) \sum_i \left(v^3_{i,max} - v^3_{i,min}\right) f(v_i)$, where i indicates each energy bin that spans in velocity space from $v_{i,min}$ to $v_{i,max}$ and $v_{i,max} = v_{i+1,min}$.

Electron impact rates

The JADE electron observations during Juno's Europa transit are taken with two 120° × ~5° field-of-view electron sensors (JADE-E), covering

a total of 240° along the plane perpendicular to Juno's spin axis. They can electrostatically deflect up to 35° towards the direction of the local magnetic field direction to capture field-aligned electrons. Electron intensities ($cm^{-2}\,sr^{-1}\,s^{-1}\,keV^{-1}$) as a function of energy E and pitch angle θ, $I(E,\theta)$, are derived from count rates. The total reaction rate γ is given by

$$\gamma = \iint I(E,\theta)\sigma(E)\,\mathrm{d}E\,\mathrm{d}\Omega = 2\pi\int_0^{\pi}\sin\theta\,\mathrm{d}\theta\int_{E_{\min}}^{E_{\max}} I(E,\theta)\sigma(E)\,\mathrm{d}E,$$

where the differential solid angle is from assuming gyrotropy. For JADE-E's energy range during the Europa fly-by, $E_{\min} = 30$ eV and $E_{\max} = 40$ keV. We estimate these reaction rates using the energy-dependent cross-sections $\sigma(E)$ for each reaction and species (Extended Data Table 3).

Since JADE-E does not measure electrons below ~30 eV, it misses a small portion of the relevant ionizing electron population below this energy. We extend the intensities below JADE-E's energy range by fitting kappa distributions to the electron intensity spectra (example given in Extended Data Fig. 2), following results from an empirical model that reproduced previous electron observations at Jupiter[55]. Integrating the above equation from $E_{\min} = 0$ eV using the empirical model intensities below 30 eV, we find reaction rates that are 10–30% larger than those solely using JADE-E's lower-energy limit of $E_{\min} = 30$ eV.

O_2^+ density determination

The JADE instrument cannot isolate species with the same mass per charge, hence the $M/q = 32$ data product contains fluxes from S^+ and O_2^+ and may also contain false coincidences from O^+ and S^{++} on the lower-energy end of the observed flux enhancements. We isolate and extract the signature of fresh O_2^+ PUIs using a data-driven method described below. Although modelling the specific instrument response to different species can be used to extract composition ratios[53], we apply a strictly data-driven approach to estimate O_2^+ densities. Since the H_2^+ ions are unambiguously local Europa-genic PUIs, their energy spectra give a data-driven representation of a nominal PUI. We assume O_2^+ PUIs will have a similar distribution, scaled up by a factor of 16 in energy due to their mass ratio to H_2^+. Therefore, we use the shape of the H_2^+ PUI distribution to apply a mask to the O_2^+ data and derive densities from this mask.

We derive a mask from the H_2^+ spectrogram by finding contours in the H_2^+ flux that occur within a certain percent of the peak for each time step. Extended Data Fig. 1b shows this mask. The rates below those of 20%, 40% and 60% from the peak flux have been masked out. From this masked data, we calculate the H_2^+ density again, finding it to be lower than that derived for the entire distribution. We then calculate the correction factor that we would need to scale the mask-derived densities to reach the correct values, as shown in Extended Data Fig. 1d. We then apply the mask to the O_2^+ dataset, scaled up in energy by a factor of 16 (Extended Data Fig. 1a), calculate the density for the masked O_2^+ dataset and then apply the same correction factor. Finally, we subtract the derived density using this method upstream of Europa at 9:39 to remove the contribution from foreground magnetospheric ions not of Europa-genic origin. The dashed orange lines in Extended Data Fig. 1c show the range of O_2^+ densities we derived for values 20–60%.

As shown in Extended Data Fig. 1a,d, the higher-energy $M/q = 32$ population very nearly tracks the energy distribution expected based on H_2^+ PUIs. Therefore, we attribute the higher-energy ions at $M/q = 32$ to fresh O_2^+ PUIs from Europa's atmosphere picked up in similar locations and conditions to H_2^+. The range of densities for O_2^+ found with this technique is shown in Fig. 1f.

PUI advection model

The PUI density at any location is determined by the net pickup upstream along the streamline intersecting that point. We employ a simple streamline model originally developed for Io's plasma interaction. The original formulation determined the velocity field as a function of the Peterson conductance Σ_1 and Alfvénic conductance Σ_A (Appendix A2 in ref. 56 and Section 2.1.2 in ref. 48). Here, we reformulate the velocity field to depend on two unknown parameters: (1) the interaction strength $\bar{\alpha} = \frac{\Sigma_1}{\Sigma_1 + 2\Sigma_A} = \frac{\delta v}{v_0}$ and (2) ionospheric distance R_I, where v_0 is the unperturbed flow speed and δv is the maximum change of the total flow speed. The plasma flow velocity vector is then given by:

$$\mathbf{v}_B = v_0\begin{bmatrix}1-\bar{\alpha}\\0\\0\end{bmatrix} \quad \text{for} \quad x_B^2 + y_B^2 \le R_I^2,$$

$$\mathbf{v}_B = v_0\begin{bmatrix}1-\bar{\alpha}R_I^2(x_B^2-y_B^2)/(x_B^2+y_B^2)^2\\-\bar{\alpha}R_I^2\,2x_By_B/(x_B^2+y_B^2)^2\\0\end{bmatrix} \quad \text{for} \quad x_B^2 + y_B^2 > R_I^2,$$

where $\mathbf{v}_B$ is in a coordinate system with $-z_B$ aligned with the magnetic field axis (at Europa, the magnetic field is predominantly in the $-z_{EPhiO}$ direction), $+x_B$ is aligned with the flow direction (as in x_{EPhiO}) and $+y_B$ completes the right-handed system, as shown in Extended Data Fig. 5. The velocity in the EPhiO coordinate system requires a single rotation about the $+x_B$ axis by angle φ with a rotation matrix, such that $\mathbf{v}_{EPhiO} = M\mathbf{v}_B$, where

$$M = \begin{bmatrix}1 & 0 & 0\\0 & \cos\varphi & \sin\varphi\\0 & -\sin\varphi & \cos\varphi\end{bmatrix}.$$

During Juno's fly-by, that angle is approximately $\varphi = 12°$ using the JRM09 internal field model[33] and current sheet model[34]. However, the resulting velocity field values are not very sensitive to changes in this angle of ~5–10°. Note that this streamline model neglects the Hall effect, which has a minor effect on the ion flow in Europa's ionosphere[15,57].

Extended Data Fig. 6 compares this two-parameter model with the in situ speeds measured by JADE for $\bar{\alpha} = (0.4, 0.55, 0.7)$ and $H_I = R_I - R_{Eur} = (30\,\mathrm{km}, 100\,\mathrm{km}, 300\,\mathrm{km})$. Three model curves are shown in each time series, corresponding to rigid corotation at 104 km s^{-1} with respect to Europa along with sub-corotation speeds of 100 and 95 km s^{-1} as reasonable possibilities[27]. Overall, we find this model successfully replicates the flow speeds and trends observed by JADE. Specifically, the model predicts a depletion in speed as Juno transits near the centre of the wake, followed by a speed enhancement as Juno encounters the sub-Jovian flank where streamlines are compressed (leading to increased plasma speed) to divert around Europa. We choose the value of $H_I = 30$ km here in our analysis as the dominantly O_2 atmosphere is understood to have a scale height of tens of kilometres[4,20], but note that the results are not very sensitive to this choice, as discussed below. For the interaction strength, we find that lower values of $\bar{\alpha} = 0.4$ underpredict the observed speed variations, whereas $\bar{\alpha} = 0.7$ overpredicts them. Hence, we use an intermediate value of $\bar{\alpha} = 0.55$ for our analysis, but as discussed below, the results are relatively insensitive to the specific choices of $\bar{\alpha}$ and H_I.

To determine the PUI density for a specific set of plasma flow and neutral atmosphere conditions, we solve the continuity equation for an advecting plasma with a source, $\frac{\partial n}{\partial t} + \nabla\cdot(n\mathbf{v}) = P$, where n is the PUI density, $\mathbf{v}$ is the plasma flow velocity from the model described above and P is the PUI injection source term. Let $P = \gamma n_a(\mathbf{r})$, where $\mathbf{r}$ is the radial vector from the centre of Europa, γ is the ionization rate and $n_a(\mathbf{r})$ is the atmospheric neutral density assuming a radially symmetric profile. Assuming the flow is in one dimension s along the streamline and that the density profile is not explicitly dependent on time, then we can

solve $v\frac{\partial n}{\partial s} = \gamma n_a(\mathbf{r})$ for the PUI density at Juno's location using finite differences along a streamline, such that $n_{i+1} = n_i + \frac{\gamma \Delta s n_a(\mathbf{r}_i)}{v_i}$. Assuming the neutral density $n_0 = 0$ far upstream and using a constant step size Δs, the local PUI density at Juno's location for a given species is then given by:

$$n = \gamma \Delta s \sum_i \frac{n_a(\mathbf{r}_i)}{v_i}.$$

We use a small step size of $\Delta s = 0.05\,R_E$, such that the results are not sensitive to this choice. The atmospheric profile considered is $n_a(r) = n_{a0}\exp(-h/H)r^{-2}$, where h is the altitude above the surface accounting for Europa's oblateness (it has an equatorial radius of 1,560.8 km and a flatness coefficient of 1.98×10^{-3}), H is the atmospheric scale height, and r is the radial distance from Europa's centre. Two additional published atmospheric profiles are also included for comparison[3,20]. We apply this advection model to the period after Juno exits Europa's geometric wake starting at 2022-272 09:36:29. The fit shown in Fig. 3 is derived using $\bar{\alpha} = 0.55$ and $H_1 = 30$ km. However, we tested the sensitivity of these results to changes in the two components in the model in the range discussed above. In this sensitivity investigation, we found the overall interpretation and extraction of atmospheric profile was highly insensitive to the choice of either parameter, with the exception of $H_1 = 300$ km. For large scale heights like 300 km, the flow would be appreciably slowed near Juno's close approach leading to a substantial perturbation in PUI densities that JADE did not observe. Hence, overall the derived results are robust to changes in the plasma interaction within a reasonable parameter space.

Atmospheric profile calculations

The column density along the radial direction for an atmospheric density profile $n_a(r)$ is $\int n_a(r)\,dr$. For an exponential altitude with scale height $H = kT/mg$, the thermal energy per kilometre scale height is 4.4×10^{-4} eV km^{-1} or 5.1 K km^{-1} for Europa's surface gravity of $g = 1.315$ m s^{-2} and Boltzmann's constant $k = 1.38 \times 10^{-23}$ m^2 s^{-2} K^{-1} = 8.6 2×10^{-5} eV K^{-1}.

Determination of H_2 and O_2 production rates

Since H_2 is more readily released from Europa's surface and gravitational well, the total H_2 production rate allows us to directly estimate the total O_2 production rate within Europa's icy surface. The O_2 mass production rate is assumed to be 8 times the H_2 production rate from the stoichiometric ratio of hydrogen and oxygen in H_2O. We determine the total H_2 production rate in Europa's icy surface using Juno's Europa fly-by data, Juno measurements of the electron characteristics in the vicinity of Europa's orbit and Juno observations of H_2^+ produced from Europa's neutral H_2 loss.

The previous estimate of total H_2 loss rate from Europa[29] did not account for PUIs directly lost from Europa and relied on Voyager/Galileo electron characteristics to determine loss rates in the vicinity of Europa's orbit. Previous reaction rate estimates[40] found that 86–91% of all reaction pathways for neutral H_2 were due to electron impacts. Therefore, we focus on updating these reactions with Juno measurements, as they are the overwhelmingly dominant reaction pathways. The recent fly-by along with Juno measurements in the vicinity of Europa's orbit allow for a direct determination of the electron impact ionization rates in both environments. We use Juno/JADE observations to improve the electron impact rate estimates and separately estimate the total losses from Europa's atmosphere versus within the neutral toroidal cloud.

First, we determine the electron distribution function for all times Juno was within 9 to 10 R_J and within 2 R_J from the magnetic equator (Extended Data Table 2). An example set of spectra is shown in Extended Data Fig. 2. We then fit the electron intensity profile as discussed in the 'Electron impact rates' in Methods and determine electron impact ionization rates for all time periods. We bin these rates by magnetic latitude (Extended Data Fig. 3) and perform a weighted average for each latitude bin by the time Europa spends in each magnetic latitude. In this way, we can determine the average electron conditions experienced by neutrals in Europa's orbit (Extended Data Fig. 4 and Extended Data Table 3) using all relevant reaction cross sections[40,58–62].

To directly estimate the total PUI loss rate from Europa's neutral atmosphere, JADE must transit streamlines that sample the majority of the neutral H_2 column density. As Juno transits streamlines down to 200–300 km within a single thermal scale height, it will sample nearly the entire neutral atmosphere. A single population with a radial dependence of $n(r) = n_0\exp(-h/\lambda)r^{-2}$ (ref. 37) is capable of completely fitting the observed PUIs. By comparison, the comprehensive neutral DSMC model[3] of the atmosphere dominated by thermal neutrals underpredicts the total PUI content. Hence, we find that a thermally dominated population of neutral H_2 is not the dominant producer of the observed H_2^+ PUIs. Given this, we conclude that the observed PUIs represent the dominant losses, enabling us to estimate the total H_2 loss.

Given the dawn-side observation we use to infer global atmospheric characteristics, we investigate two cases to bound this estimate: (1) a radially symmetric atmosphere and (2) a case where the neutral H_2 dawn/dusk asymmetry is a factor of 2, which is the upper limit of the dawn/dusk column densities observed in O_2 by the Hubble Space Telescope[4,11]. We use the time range of 9:37 to 9:39 as representative upstream conditions, such that the average upstream electron impact ionization reaction rate is 3.4×10^{-6} s^{-1}. We further assume that half of the H_2 neutrals in the downstream hemisphere experience a median reaction rate of 5.2×10^{-6} s^{-1} from the wake (Extended Data Fig. 4). Combining these two rates, we derive a local-time-averaged reaction rate of 4.3×10^{-6} s^{-1}. Using our derived electron impact ionization rates to integrate over Europa's entire atmosphere in these cases, the resulting estimate is 0.14 ± 0.03 kg s^{-1} of direct H_2^+ PUI loss.

From our updated electron reaction rates, along with existing non-electron-related rates[40], we find that electron impact ionization, $H_2 + e^- \rightarrow H_2^+ + 2e^-$, leads to 41–58% of total H_2 losses in Europa's orbit away from the moon, whereas 54–58% of H_2 losses occur in the immediate vicinity of Europa. A production rate of 0.7 ± 0.3 kg s^{-1} of charged H_2^+ was derived from H_2^+ observations throughout Jupiter's magnetosphere[29]. We now discriminate between H_2^+ directly lost from Europa's atmosphere exposed to higher electron impact ionization rates with those picked up from Europa's neutral H_2 toroidal cloud. From the Europa fly-by, we estimate 0.16 ± 0.04 kg s^{-1} of these PUIs are directly picked up in the immediate vicinity of Europa from its atmospheric neutral H_2. This leaves 0.54 ± 0.34 kg s^{-1} of ions to be produced from Europa's neutral toroidal cloud. Using the relative fraction of impact ionization found here, 0.29 ± 0.09 kg s^{-1} of neutral H_2 is lost directly from the Europa's atmosphere due to H_2 reactions, whereas the majority of neutral loss is from the torus and estimated to be 1.20 ± 0.72 kg s^{-1}. The total estimated loss rate for H_2 is then 1.5 ± 0.8 kg s^{-1}. Using stoichiometric ratios for water, the total O_2 production rate is then 12 ± 6 kg s^{-1}.

Independently, the altitude profile of $n(r) = n_0\exp(-h/\lambda)r^{-2}$ can be used to estimate the total neutral H_2 outflow. The length scale over which neutral losses occur can be interpreted to be $\lambda = w/L$, where w is the average neutral outflow speed and L is the total reaction rate for H_2. For the total reaction rate, we follow a similar analysis as above. Averaging the upstream and wake electron impact ionization rates gives an average value that is ~80% of the wake value. Therefore, we sum all reaction rates derived for the H_2 in the third column of Extended Data Table 3 for the wake and multiply by 80% to determine the average value of these electron-driven rates to be 3.8–11 × 10^{-6} s^{-1}. We additionally estimate from the second column in this table that non-electron-driven rates can contribute an additional 20%, so we estimate a total H_2 reaction rate of 4.6–13 × 10^{-6} s^{-1}. The outflow speed is then $w = 58 \pm 34$ m s^{-1}. To estimate the total loss rate with this outflow approximation, we similarly assume that the surface density is either

azimuthally symmetric with $n_0 = 1.8 \pm 0.05 \times 10^5$ cm^{-3} or has a dawn/dusk asymmetry of 2 with an average surface density of $n_0 = 2.7 \pm 0.08 \times 10^5$ cm^{-3}. The total neutral loss rate estimate is then $4\pi R_E^2 n_0 w = 1.5 \pm 1.1$ kg s^{-1}, which is remarkably similar to our higher-fidelity estimate of 1.5 ± 0.8 kg s^{-1} above, which was estimated in a completely different way using years of Juno observations of Europa-genic H_2^+ PUIs throughout the magnetosphere.

Data availability

The JNO-J/SW-JAD-3-CALIBRATED-V1.0 data presented in this manuscript, https://doi.org/10.1007/s11214-013-9990-9, can be obtained from the Planetary Data System (PDS) at https://pds-ppi.igpp.ucla.edu/mission/JUNO/JNO/JAD. Source data are provided with this paper.

References

1. Johnson, R. E. *Energetic Charged-Particle Interactions with Atmospheres and Surfaces* (Springer, 1990).
2. Johnson, R. E. et al. The origin and fate of O_2 in Europa's ice: an atmospheric perspective. *Space Sci. Rev*. https://doi.org/10.1007/s11214-019-0582-1 (2019).
3. Smyth, W. H. & Marconi, M. L. Europa's atmosphere, gas tori, and magnetospheric implications. *Icarus* **181**, 510–526 (2006).
4. Oza, A. V., Johnson, R. E. & Leblanc, F. Dusk/dawn atmospheric asymmetries on tidally-locked satellites: O_2 at Europa. *Icarus* **305**, 50–55 (2018).
5. Davis, M. R., Meier, R. M., Cooper, J. F. & Loeffler, M. J. The contribution of electrons to the sputter-produced O_2 exosphere on Europa. *Astrophys. J. Lett*. **908**, L53 (2021).
6. Nordheim, T. A. et al. Magnetospheric ion bombardment of Europa's surface. *Planet. Sci. J.* **3**, 5 (2022).
7. Addison, P., Liuzzo, L. & Simon, S. Effect of the magnetospheric plasma interaction and solar illumination on ion sputtering of Europa's surface ice. *J. Geophys. Res. Space Phys*. **127**, e2021JA030136 (2022).
8. Roth, L. et al. Detection of a hydrogen corona in HST Lyα images of Europa in transit of Jupiter. *Astron. J.* **153**, 67 (2017).
9. Hall, D. T., Strobel, D. F., Feldman, P. D., McGrath, M. A. & Weaver, H. A. Detection of an oxygen atmosphere on Jupiter's moon Europa. *Nature* **373**, 677–679 (1995).
10. Hansen, C. J., Shemansky, D. E. & Hendrix, A. R. Cassini UVIS observations of Europa's oxygen atmosphere and torus. *Icarus* **176**, 305–315 (2005).
11. Roth, L. et al. Europa's far ultraviolet oxygen aurora from a comprehensive set of HST observations. *J. Geophys. Res. Space Phys*. **121**, 2143–2170 (2016).
12. de Kleer, K., Milby, Z., Schmidt, C., Camarca, M. & Brown, M. E. The optical aurorae of Europa, Ganymede, and Callisto. *Planet. Sci. J.* **4**, 37 (2023).
13. Paganini, L. et al. A measurement of water vapour amid a largely quiescent environment on Europa. *Nat. Astron.* **4**, 266–272 (2020).
14. Roth, L. A stable H_2O atmosphere on Europa's trailing hemisphere from HST images. *Geophys. Res. Lett.* **48**, e94289 (2021).
15. Saur, J., Strobel, D. F. & Neubauer, F. M. Interaction of the Jovian magnetosphere with Europa: constraints on the neutral atmosphere. *J. Geophys. Res.* **103**, 19947–19962 (1998).
16. Harris, C. D. K., Jia, X. & Slavin, J. A. Multi-fluid MHD simulations of Europa's plasma interaction: effects of variation in Europa's atmosphere. *J. Geophys. Res. Space Phys*. **127**, e2022JA030569 (2022).
17. Cervantes, S. & Saur, J. Constraining Europa's subsolar atmosphere with a joint analysis of HST spectral images and Galileo magnetic field data. *J. Geophys. Res. Space Phys*. **127**, e2022JA030472 (2022).
18. Blöcker, A., Saur, J. & Roth, L. Europa's plasma interaction with an inhomogeneous atmosphere: development of Alfvén winglets within the Alfvén wings. *J. Geophys. Res. Space Phys*. **121**, 9794–9828 (2016).
19. Dols, V. J., Bagenal, F., Cassidy, T. A., Crary, F. J. & Delamere, P. A. Europa's atmospheric neutral escape: importance of symmetrical O_2 charge exchange. *Icarus* **264**, 387–397 (2016).
20. Vorburger, A. & Wurz, P. Europa's ice-related atmosphere: the sputter contribution. *Icarus* **311**, 135–145 (2018).
21. Teolis, B. D., Wyrick, D. Y., Bouquet, A., Magee, B. A. & Waite, J. H. Plume and surface feature structure and compositional effects on Europa's global exosphere: preliminary Europa mission predictions. *Icarus* **284**, 18–29 (2017).
22. Paterson, W. R., Frank, L. A. & Ackerson, K. L. Galileo plasma observations at Europa: ion energy spectra and moments. *J. Geophys. Res. Space Phys*. **104**, 22779–22791 (1999).
23. Volwerk, M., Kivelson, M. G. & Khurana, K. K. Wave activity in Europa's wake: implications for ion pickup. *J. Geophys. Res. Space Phys*. **106**, 26033–26048 (2001).
24. Bagenal, F. & Dols, V. The space environment of Io and Europa. *J. Geophys Res. Space Phys*. **125**, 8241–8257 (2020).
25. Bolton, S. J. et al. The Juno mission. *Space Sci. Rev.* **213**, 5–37 (2017).
26. McComas, D. J. et al. The Jovian Auroral Distributions Experiment (JADE) on the Juno mission to Jupiter. *Space Sci. Rev.* **213**, 547–643 (2017).
27. Bagenal, F., Wilson, R. J., Siler, S., Paterson, W. R. & Kurth, W. S. Survey of Galileo plasma observations in Jupiter's plasma sheet. *J. Geophys. Res. Planets* **121**, 871–894 (2016).
28. Jia, X., Kivelson, M. G., Khurana, K. K. & Kurth, W. S. Evidence of a plume on Europa from Galileo magnetic and plasma wave signatures. *Nat. Astron.* **2**, 459–464 (2018).
29. Szalay, J. R. et al. Water-group pickup ions from Europa-genic neutrals orbiting Jupiter. *Geophys. Res. Lett.* **49**, e2022GL098111 (2022).
30. Allegrini, F. et al. Plasma observations during the June 7, 2021 Ganymede flyby from the Jovian Auroral Distributions Experiment (JADE) on Juno. *Geophys. Res. Lett.* **49**, e2022GL098682 (2022).
31. Sittler, E. C. et al. Plasma ion composition measurements for Europa. *Planet. Space Sci.* **88**, 26–41 (2013).
32. Desai, R. T. et al. Cassini CAPS identification of pickup ion compositions at Rhea. *Geophys. Res. Lett.* **45**, 1704–1712 (2018).
33. Connerney, J. E. P. et al. A new model of Jupiter's magnetic field From Juno's first nine orbits. *Geophys. Res. Lett.* **45**, 2590–2596 (2018).
34. Connerney, J. E. P., Timmins, S., Herceg, M. & Joergensen, J. L. A Jovian magnetodisc model for the Juno era. *J. Geophys. Res. Space Phys*. **125**, e28138 (2020).
35. Kliore, A. J., Hinson, D. P., Flasar, F. M., Nagy, A. F. & Cravens, T. E. The ionosphere of Europa from Galileo radio occultations. *Science* **277**, 355–358 (1997).
36. Westlake, J. H. et al. The Plasma Instrument for Magnetic Sounding (PIMS) on the Europa Clipper mission. *Space Sci. Rev.* **219**, 62 (2023).
37. Summers, M. E., Strobel, D. F., Yung, Y. L., Trauger, J. T. & Mills, F. The structure of Io's thermal corona and implications for atmospheric escape. *Astrophys. J.* **343**, 468 (1989).
38. Mauk, B. H., Mitchell, D. G., Krimigis, S. M., Roelof, E. C. & Paranicas, C. P. Energetic neutral atoms from a trans-Europa gas torus at Jupiter. *Nature* **421**, 920–922 (2003).
39. Lagg, A., Krupp, N., Woch, J. & Williams, D. J. In-situ observations of a neutral gas torus at Europa. *Geophys. Res. Lett.* **30**, 1556 (2003).
40. Smith, H. T., Mitchell, D. G., Johnson, R. E., Mauk, B. H. & Smith, J. E. Europa neutral torus confirmation and characterization based on observations and modeling. *Astrophys. J.* **871**, 69 (2019).

41. Marconi, M. L. A kinetic model of Ganymede's atmosphere. *Icarus* **190**, 155–174 (2007).
42. Carberry Mogan, S. R. et al. Callisto's atmosphere: first evidence for H_2 and constraints on H_2O. *J. Geophys. Res. Planets* **127**, e2022JE007294 (2022).
43. Spencer, J. R., Tamppari, L. K., Martin, T. Z. & Travis, L. D. Temperatures on Europa from Galileo photopolarimeter-radiometer: nighttime thermal anomalies. *Science* **284**, 1514–1516 (1999).
44. Krüger, H., Krivov, A. V., Sremčević, M. & Grün, E. Impact-generated dust clouds surrounding the Galilean moons. *Icarus* **164**, 170–187 (2003).
45. Costello, E. S., Phillips, C. B., Lucey, P. G. & Ghent, R. R. Impact gardening on Europa and repercussions for possible biosignatures. *Nat. Astron.* **5**, 951–956 (2021).
46. Nordheim, T. A., Hand, K. P. & Paranicas, C. Preservation of potential biosignatures in the shallow subsurface of Europa. *Nat. Astron.* **2**, 673–679 (2018).
47. Strobel, D. F., Zhu, X. & Summers, M. E. On the vertical thermal structure of Io's atmosphere. *Icarus* **111**, 18–30 (1994).
48. Saur, J., Grambusch, T., Duling, S., Neubauer, F. M. & Simon, S. Magnetic energy fluxes in sub-Alfvénic planet star and moon planet interactions. *Astron. Astrophys.* **552**, A119 (2013).
49. Plainaki, C. et al. Towards a global unified model of Europa's tenuous atmosphere. *Space Sci. Rev.* **214**, 40 (2018).
50. Chyba, C. F. Energy for microbial life on Europa. *Nature* **403**, 381–382 (2000).
51. Hand, K. P., Carlson, R. W. & Chyba, C. F. Energy, chemical disequilibrium, and geological constraints on Europa. *Astrobiology* **7**, 1006–1022 (2007).
52. Greenberg, R. Transport rates of radiolytic substances into Europa's ocean: implications for the potential origin and maintenance of life. *Astrobiology* **10**, 275–283 (2010).
53. Kim, T. K. et al. Method to derive ion properties from Juno JADE including abundance estimates for O^+ and and S^{2+}. *J. Geophys. Res. Space Phys.* **125**, e026169 (2020).
54. McComas, D. J. et al. Interstellar pickup ion observations halfway to the termination shock. *Astrophys. J. Suppl. Ser.* **254**, 19 (2021).
55. Jun, I., Garrett, H. B., Cassidy, T. A., Kim, W. & Dougherty, L. Updating the Jovian electron plasma environment. *IEEE Trans. Plas. Sci.* **47**, 3915–3922 (2019).
56. Saur, J., Neubauer, F. M., Strobel, D. F. & Summers, M. E. Three-dimensional plasma simulation of Io's interaction with the Io plasma torus: asymmetric plasma flow. *J. Geophys. Res. Space Phys.* **104**, 25105–25126 (1999).
57. Hartkorn, O. & Saur, J. Induction signals from Callisto's ionosphere and their implications on a possible subsurface ocean. *J. Geophys. Res. Space Phys.* **122**, 11677–11697 (2017).
58. Straub, H. C., Renault, P., Lindsay, B. G., Smith, K. A. & Stebbings, R. F. Absolute partial cross sections for electron-impact ionization of H_2, N_2, and O_2 from threshold to 1000 eV. *Phys. Rev. A* **54**, 2146–2153 (1996).
59. Chung, S., Lin, C. C. & Lee, E. T. P. Dissociation of the hydrogen molecule by electron impact. *Phys. Rev. A* **12**, 1340–1349 (1975).
60. Itikawa, Y. Cross sections for electron collisions with oxygen molecules. *J. Phys. Chem. Ref. Data* **38**, 1–20 (2009).
61. Johnson, R. E., Cooper, P. D., Quickenden, T. I., Grieves, G. A. & Orlando, T. M. Production of oxygen by electronically induced dissociations in ice. *J. Chem. Phys.* **123**, 184715 (2005).
62. Cosby, P. C. Electron-impact dissociation of oxygen. *J. Chem. Phys.* **98**, 9560–9569 (1993).
63. Carberry Mogan, S. R., Johnson, R. E., Vorburger, A. & Roth, L. Electron impact ionization in the icy Galilean satellites' atmospheres. *Eur. Phys. J. D.* **77**, 26 (2023).

Acknowledgements

We thank the many JADE and Juno team members who made these observations possible. We thank M. Imai for producing the magnetic field line integrations. We thank H. Krüger for discussions on the Galileo dust observations, V. Dols for discussions relating to Europa's magnetospheric interaction and Y. Sarkango for magnetic field model estimates. We acknowledge NASA Juno contract NNM06AA75C and NASA New Frontiers Data Analysis Program grant 80NSSC21K0823. S.F. acknowledges support from the Swedish Research Council (Grant No. 2018-03454) and the Swedish National Space Agency (Grant No. 115/18). J.S. acknowledges funding from the European Research Council under the European Union's Horizon 2020 research and innovation programme (Grant Agreement No. 884711). A part of the research was carried out at the Jet Propulsion Laboratory, California Institute of Technology, under a contract with NASA (80NM0018D0004).

Author contributions

J.R.S. wrote the manuscript and performed the data analysis. All authors contributed to the interpretation of the results. D.J.M. led the design and development of the JADE instrument on which the study is based. F.A., R.W.E., F.B., D.J.M. and R.J.W. contributed to the JADE analysis, interpretation and background subtraction discussion. J.S., H.T.S., A.V. and S.F. contributed to the electron impact ionization and PUI generation analysis. J.S. and D.S. contributed to the streamline and neutral atmosphere modelling. S.V. contributed to the subsurface ocean chemistry discussion. S.J.B. is the principal investigator of the mission.

Competing interests

The authors declare no competing interests.

Additional information

Extended data Extended data are available for this paper at https://doi.org/10.1038/s41550-024-02206-x.

Supplementary information The online version contains supplementary material available at https://doi.org/10.1038/s41550-024-02206-x.

Correspondence and requests for materials should be addressed to J. R. Szalay.

Peer review information *Nature Astronomy* thanks Orenthal Tucker and the other, anonymous, reviewer(s) for their contribution to the peer review of this work.

https://doi.org/10.1038/s41550-024-02206-x

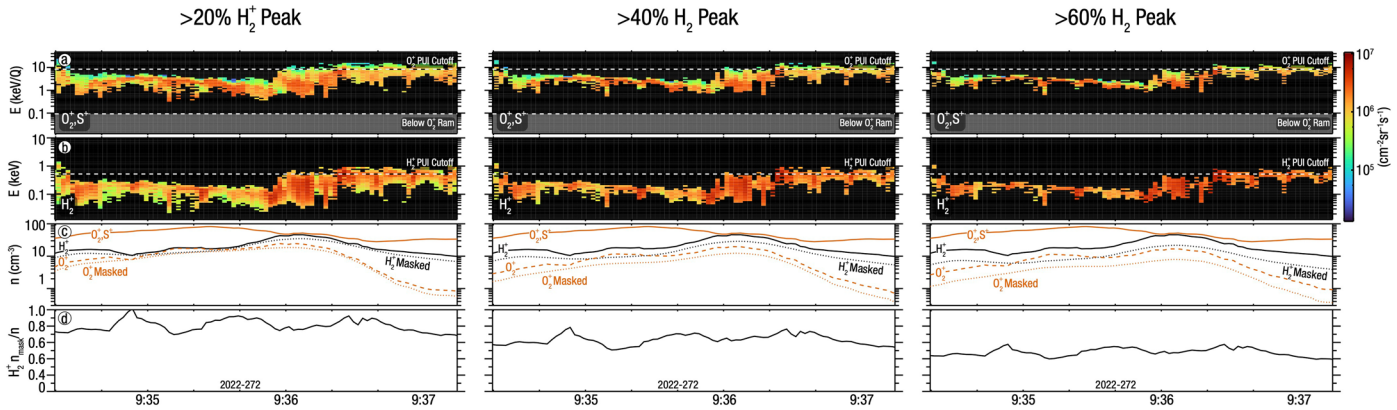

Extended Data Fig. 1 | Masking analysis for O_2^+ density estimation. Panels (a) and (b) show identical data in panels (a) and (c) in Fig. 1, where a mask has been applied to each determined by the percentage from peak flux in H_2^+. The time range shown is 2022-272 9:34:20 to 9:37:15, where modified M/q = 32 fluxes were observed above the background magnetospheric heavy ions. Panel (c) shows the densities derived solely from the masked data (dotted lines) and those corrected for the missing portion of the distribution (dashed lines) using the correction factor shown in panel (d) from H_2^+.

https://doi.org/10.1038/s41550-024-02206-x

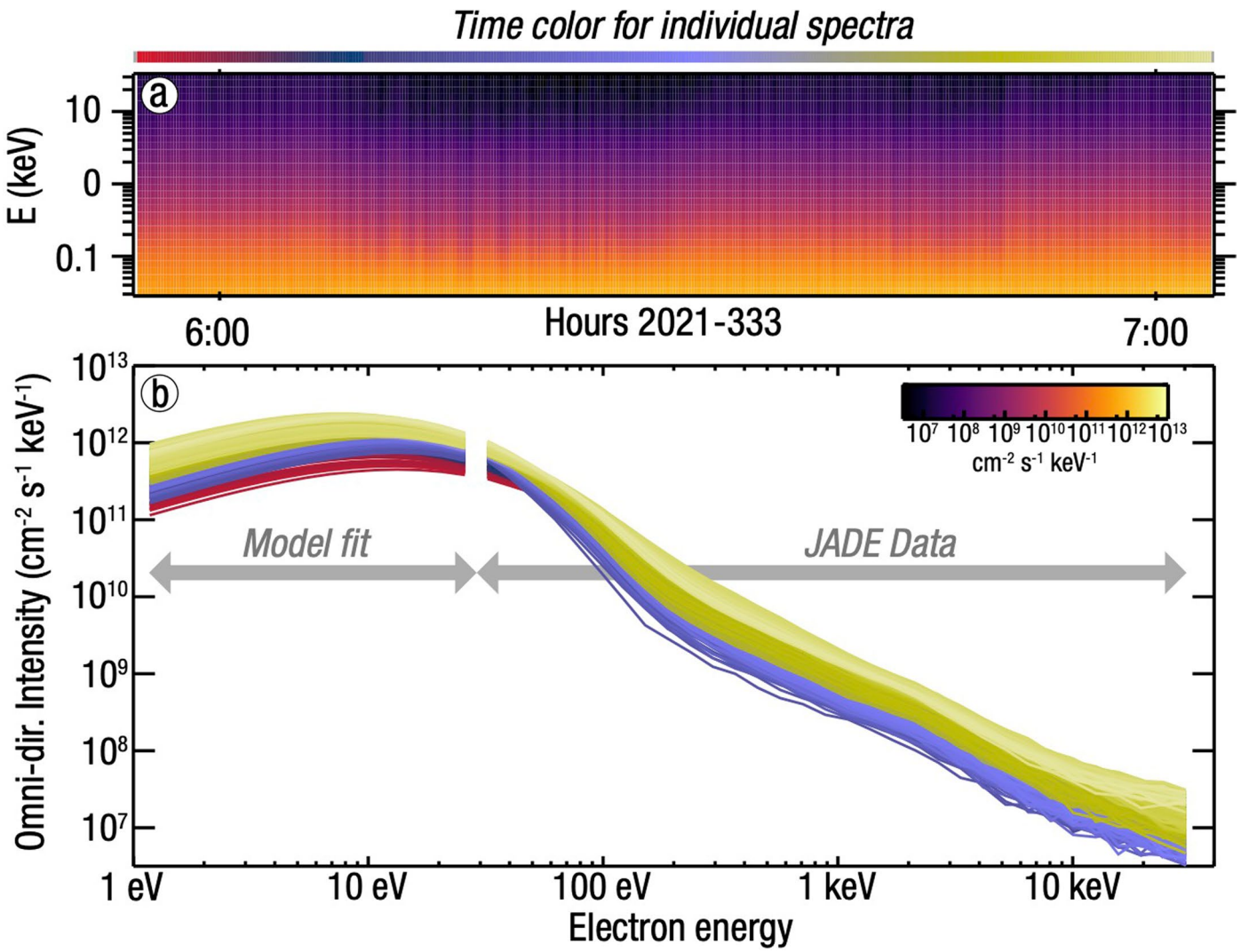

Extended Data Fig. 2 | Electron intensity distribution for electron reaction rates. Panel (a) shows example electron spectra when Juno was between r = 9-10 R_J and within z = 2 R_J from the magnetic equator during the 38th perijove. Panel (b) shows these spectra along with the extrapolated lower energy component of the distribution function by fitting each individual spectrum to a kappa distribution. These extrapolations are used to compute the full electron reaction rate cross-sections.

https://doi.org/10.1038/s41550-024-02206-x

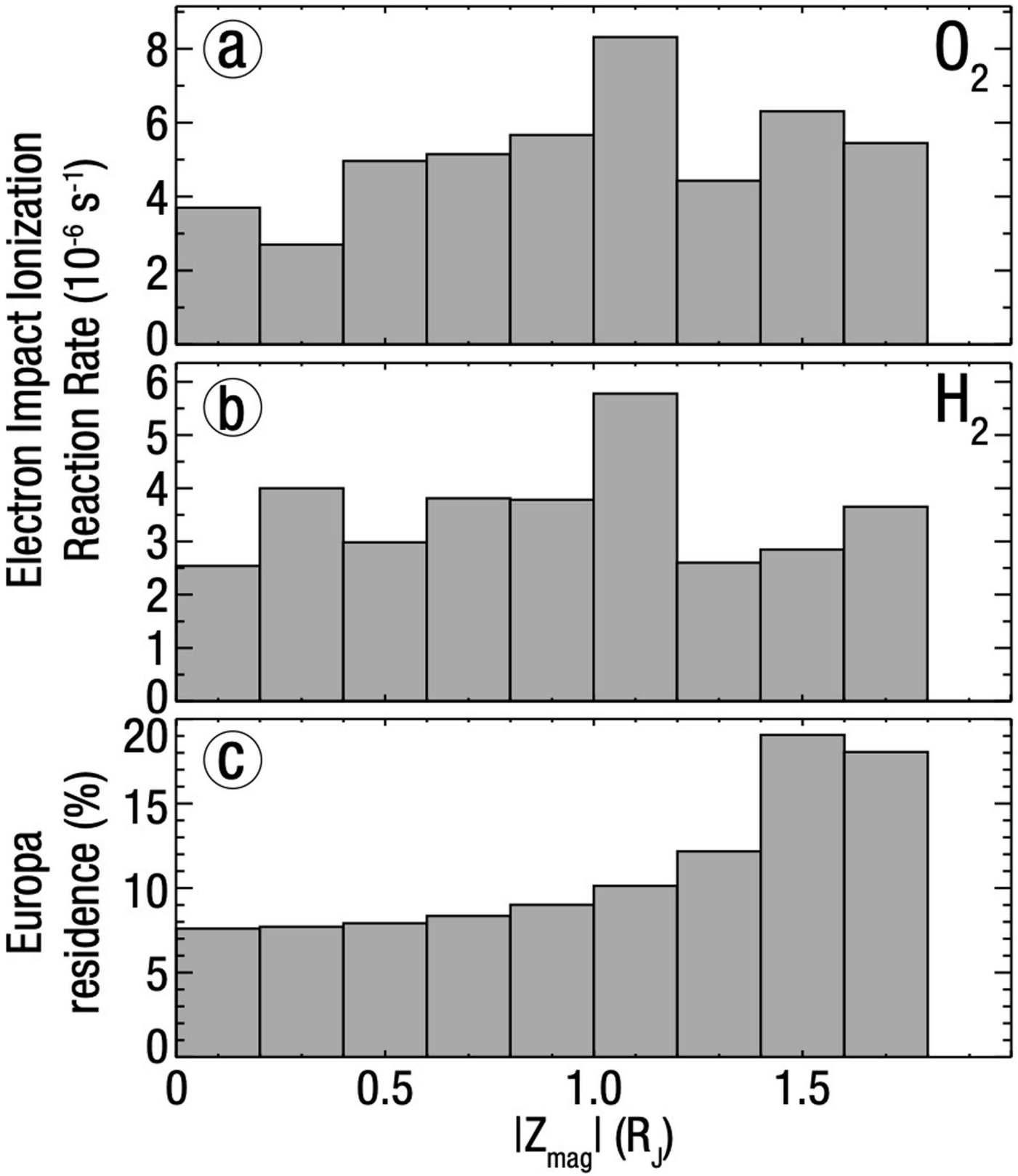

Extended Data Fig. 3 | Electron impact ionization rates for H_2 and O_2 as a function of z_{mag}. Panels (a) and (b) show the average electron impact ionization rates for each separate species derived from Juno/JADE electron measurements in the vicinity of Europa's orbit (r = 9-10 R_J and within z = 2 R_J). Panel (c) shows the relative residence time Europa spends in each location. These distributions are used to determine the normalized rates in Extended Data Fig. 4.

https://doi.org/10.1038/s41550-024-02206-x

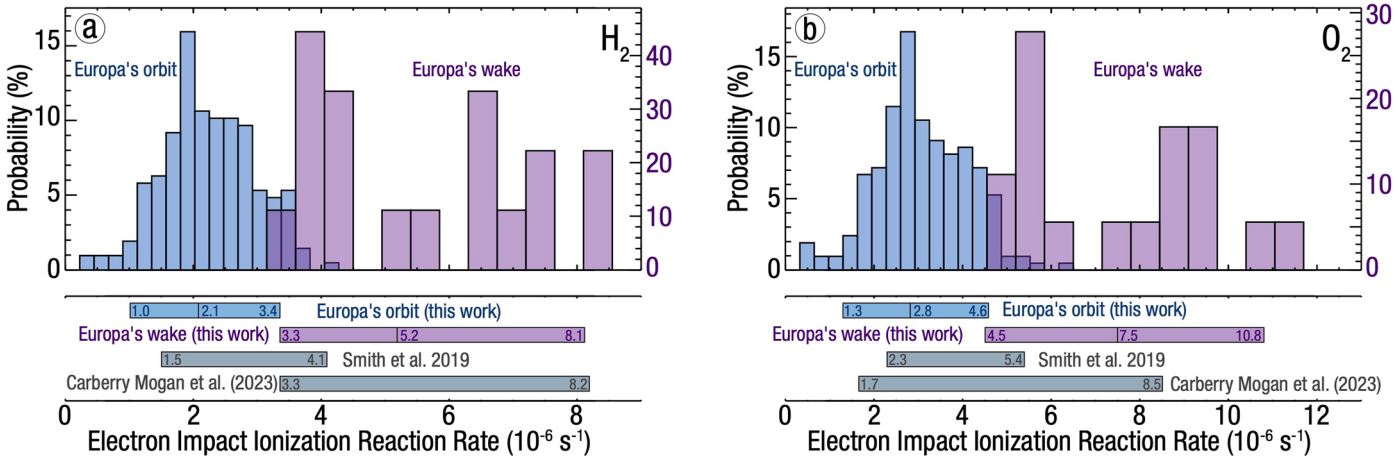

Extended Data Fig. 4 | Electron impact ionization rates for H_2 and O_2. Panels (a) and (b) show the same information for separate species. The blue histogram shows the probability distribution of total electron impact ionization rates derived from Juno/JADE electron measurements in the vicinity of Europa's orbit ($r = 9\text{-}10\ R_J$ and within $Z_{mag} \leq 2\ R_J$) normalized by time Europa spends as a function of magnetic latitude. The purple histogram shows these values derived when Juno was within Europa's geometric wake. Widths of the blue and purple bars at the bottom indicate the 10% and 90% percentiles with the median value shown in the central vertical line. Previous estimates in the vicinity of Europa's orbit are shown in grey[40,63].

https://doi.org/10.1038/s41550-024-02206-x

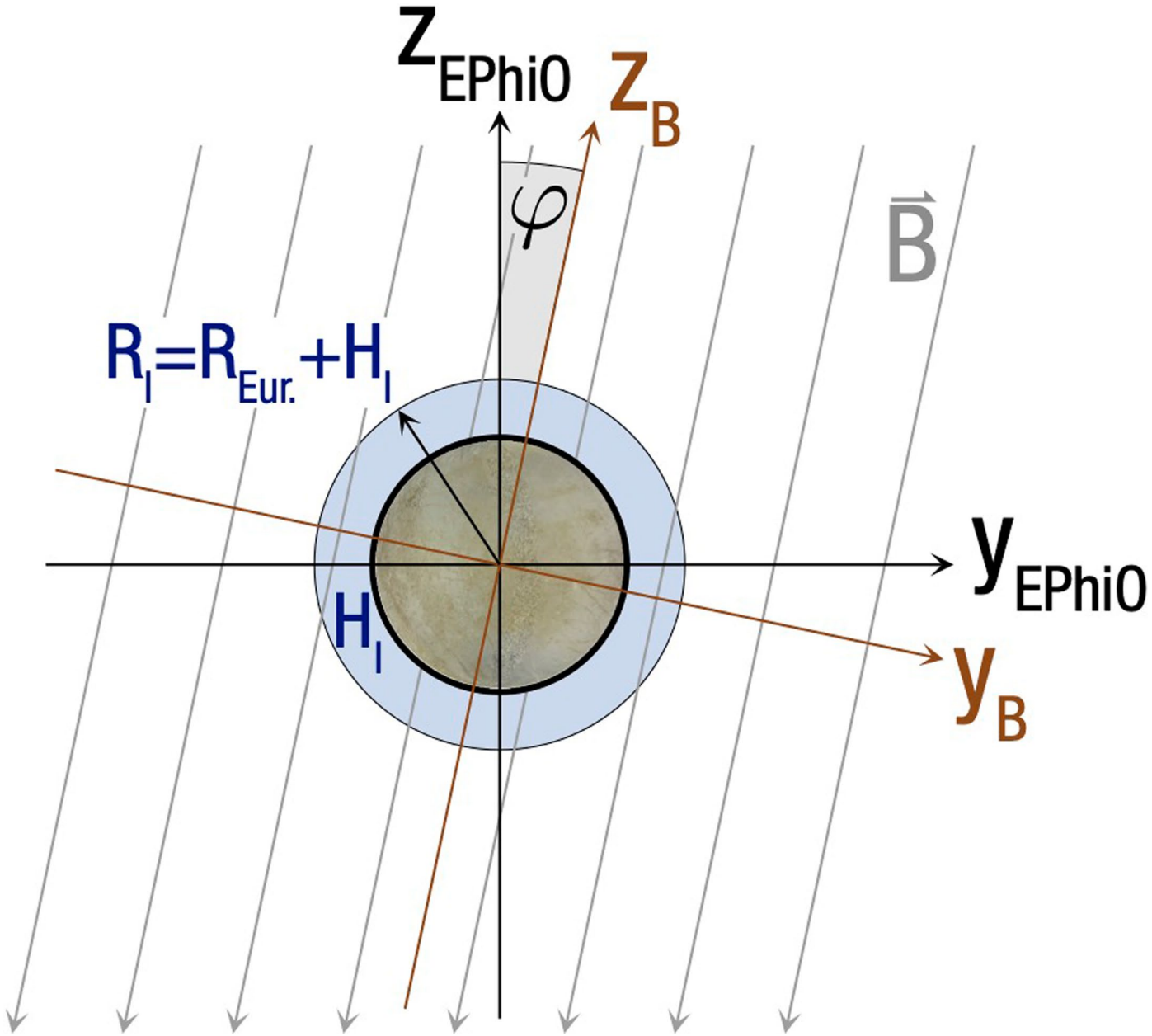

Extended Data Fig. 5 | Coordinate systems used to calculate streamlines. Orange axes show the coordinate system where $-z_B$ is aligned with the magnetic field direction and the component of B out of the page is considered negligible. This coordinate system differs from EPhiO by a rotation by angle φ about the x direction. The ionospheric altitude H_I and radius R_I are also indicated.

https://doi.org/10.1038/s41550-024-02206-x

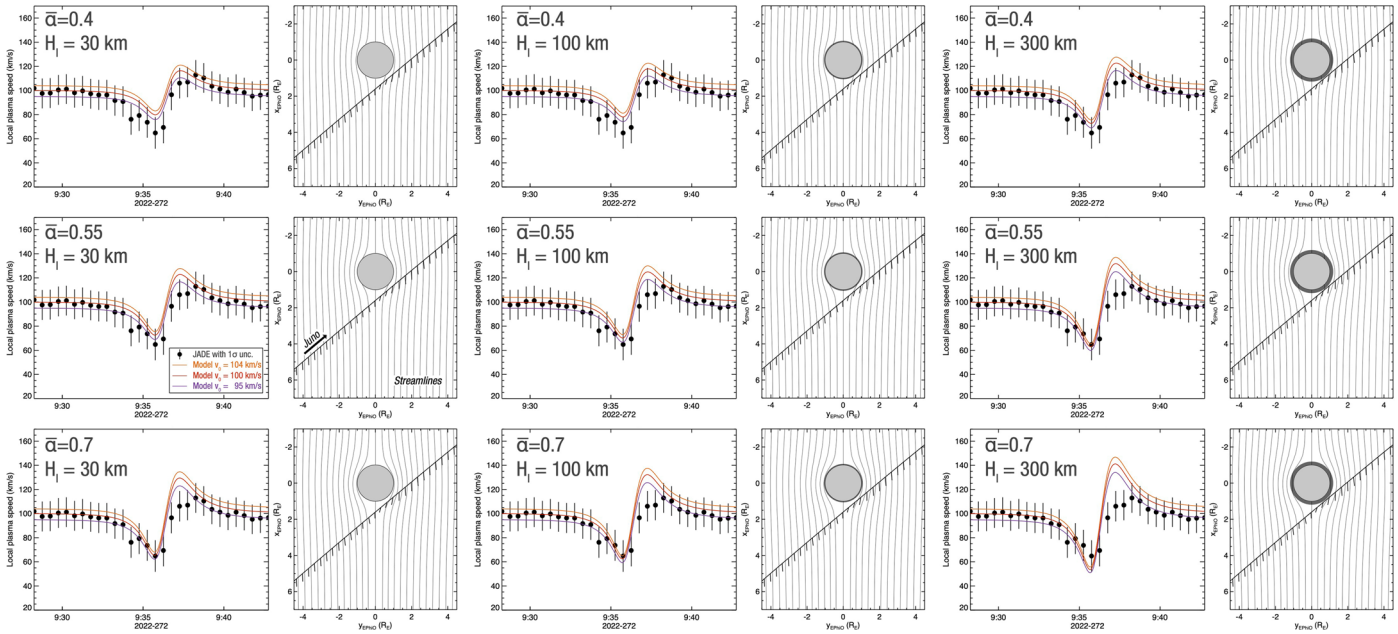

Extended Data Fig. 6 | Comparison of JADE plasma flow speeds with streamline model. Each time series panel shows the Juno/JADE derived mean local speed using JADE proton measurements along with the 1σ uncertainties summed in quadrature from values within the JADE data files. The three curves show model predictions for this speed for corotation speeds of 104 km s^{-1} (orange, rigid corotation), 100 km s^{-1} (red), and 95 km s^{-1} (purple). The panel to the right of each time series shows the corresponding streamline model along with Juno's trajectory and observed velocity vectors. The light grey circle corresponds to Europa and the dark grey annulus corresponds to the modeled ionospheric height H_I. Nine different model cases are shown for interaction strength α = (0.4,0.55,0.7) and H_I = (30 km, 100 km, 300 km). We use values of α = 0.55 and H_I = 30 throughout the analysis (middle row, left column).

https://doi.org/10.1038/s41550-024-02206-x

Extended Data Table 1 | Relevant orbital and plasma parameters at close approach

C/A Time	2022-272 9:36:29
C/A Distance	1.2 R_E
C/A Altitude	353 km
Assumed upstream |B|	440 nT
Rigid corotation speed	117 km s^{-1}
Orbital speed	13.8 km s^{-1}
Rigid corotation speed wrt. Europa	104 km s^{-1}
Juno speed wrt. Europa	23.6 km s^{-1}
H_2^+ PUI gyroradius	5 km
O_2^+ PUI gyroradius	80 km
Sys. III W. Longitude	136°
Centrifugal latitude	2.8°
Magnetic Latitude	4.1°

All parameters calculated at Juno's close approach on 2022-272 9:36:29.

https://doi.org/10.1038/s41550-024-02206-x

Extended Data Table 2 | Times used for the electron rates derivations

Perijove	Start time (UTC)	Stop time (UTC)
36	2021-245T14:23:50	2021-245T15:32:46
37	2021-289T08:54:43	2021-289T10:03:39
38	2021-333T05:54:43	2021-333T07:03:29
39	2022-012T02:14:18	2022-012T03:23:03
41	2022-099T07:30:38	2022-099T08:39:24
42	2022-142T17:57:07	2022-142T19:06:02
43	2022-186T00:58:37	2022-186T02:07:23
44	2022-229T06:26:47	2022-229T07:35:42
45	2022-272T08:51:24	2022-272T10:00:30
46	2022-310T13:18:26	2022-310T14:27:42

Time ranges are when Juno was within 9-10 R_J radial distance from Jupiter and within 2 R_J vertical distance from the magnetic equator.

https://doi.org/10.1038/s41550-024-02206-x

Extended Data Table 3 | Electron reaction rates determined by Juno/JADE observations

Reaction	Europa's Orbit (s^{-1})	Europa's Wake (s^{-1})	Cross Section
$H_2 + e^- \rightarrow H_2^+ + 2e^-$	$1.0\text{-}3.4 \times 10^{-6}$	$3.3\text{-}8.1 \times 10^{-6}$	Ref. 58
$H_2 + e^- \rightarrow H^+ + H + 2e^-$	$0.46\text{-}1.7 \times 10^{-7}$	$1.4\text{-}3.8 \times 10^{-7}$	Ref. 58
$H_2 + e^- \rightarrow H + H + e^-$	$0.37\text{-}2.0 \times 10^{-6}$	$1.4\text{-}5.0 \times 10^{-6}$	Ref. 59
H_2 reactions not involving electrons	$0.23\text{-}1.2 \times 10^{-6}$	--	Ref. 40
$O_2 + e^- \rightarrow O_2^+ + 2e^-$	$1.3\text{-}4.6 \times 10^{-6}$	$4.5\text{-}10.8 \times 10^{-6}$	Ref. 60
$O_2 + e^- \rightarrow O^+ + O + 2e^-$	$0.22\text{-}1.9 \times 10^{-6}$	$1.2\text{-}3.9 \times 10^{-6}$	Ref. 60
$O_2 + e^- \rightarrow O^{++} + O + 3e^-$	$0.054\text{-}1.8 \times 10^{-8}$	$0.79\text{-}2.3 \times 10^{-8}$	Ref. 60
$O_2 + e^- \rightarrow O + O + e^-$	$0.56\text{-}2.6 \times 10^{-6}$	$2.4\text{-}6.3 \times 10^{-6}$	Ref. 62
O_2 reactions not involving electrons	$1.2\text{-}5.4 \times 10^{-6}$	--	Ref. 40

Rates calculated both in the vicinity of Europa's orbit and within Europa's wake during Juno's Europa flyby.